17th European Rotorcraft Forum
September 24-26, 1991 Berlin, Germany

SEVENTEENTH EUROPEAN ROTORCRAFT FORUM

Paper No. 91-43

TRIMMING ROTOR BLADES WITH PERIODICALLY DEFLECTING TRAILING EDGE FLAPS

Y. K. YILLIKÇI
Undersecrateriat For Defence Industries
Ministry of National Defence
Ankara, Turkiye

SEPTEMBER 24 - 26, 1991

Berlin, Germany

Deutsche Gesellschaft für Luft- und Raumfahrt e. V. (DGLR)
Godesberger Allee 70, Bonn 2, Germany

17th European Rotorcraft Forum
September 24-26, 1991 Berlin, Germany

TRIMMING ROTOR BLADES WITH PERIODICALLY DEFLECTING TRAILING EDGE FLAPS

Y. K. YILLIKCI*
Undersecrateriat for Defence Industries
Ministery of National Defence
Ankara, Turkiye

ABSTRACT

A simplified trimming process for rotors with periodic trailing edge flap motions is developed. In this process, first collective and cyclic pitch control inputs are calculated by the use of standard helicopter trim equations. At the second stage, pitch motions are replaced with periodic trailing edge flap (TEF) motions represented up to the first harmonics. For the TEF case only rigid collective and pretwist angles are retained. The trailing edge flap motion harmonics are calculated based on the idea that TEF control must achieve identical trust harmonics of the pitch control case. Sample results for a small remotely controlled helicopter configuration with trailing edge flap controls are presented. Different flap geometries are investigated and ETF concept is evaluated.

INTRODUCTION

As known, the helicopter rotor blades are subject to a quite complicated aerodynamic environment compared with the fixed wings aerodynamics. In forward flight, additional to the velocity due to its own rotation, rotor blades sees a component of the helicopter forward velocity. On the retreating side of the disk the velocity of the blade is decreased by the forward speed. For a constant angle of attack of the blade, the varying dynamic pressure of the rotor blade aerodynamic environment in forward flight will result in producing less lift on the retreating side than on the advancing side. As the result of this phenomena a rolling moment on the rotor hub is produced. This problem is solved by introducing a cyclic varying pitch control to the blade rigid motion. The control inputs usually consists of the just the mean and first harmonics as shown below:

$$\theta = \theta_0 + \theta_{1S}\sin\psi + \theta_{1C}\cos\psi \qquad (1)$$

The mean angle θ_0 is called the collective pitch and the 1/rev harmonics θ_{1S} and θ_{1C} are called the cyclic pitch angles. Primarily, collective pitch controls the average blade force while cyclic pitch controls θ_{1S} and θ_{1C} controls the thrust vector orientation in longitudial and lateral directions respectively. To produce the collective and cyclic pitch changes on the rotor blade, a mechanical system called " swashplate " is used in standard rotor blade hub configuration.

Along with the other developments in rotary wing technologies; rotor blades with circulation controlled elliptic airfoils are being suggested as alternative rotor systems. Azimuthal and spanwise lift changes are aimed to be generated by the air jets pulsed from the trailing edge References 1,2,3,4. As for the primary application, circulation controlled rotor system planned to be applied in the X wing (stopped rotor) case to combine VTOL, hovering capabilities of rotary wing; and low speed manoeuvrability of rotary wings with the higher forward flight efficiencies at high speeds as fixed wing configuration Circulation controlled airfoils are currently at the development stage and for practical applications they require complicated pneomatic control systems to generate and manipulate the required leading and trailing edge air jet pulses.

On the other hand, unmanned air vehicles have been found applications both in military and civilian areas in recent years. For future UAV applications, designers started to search for new, unconventional UAV configurations. For specific mission and performance requirements, configurations which are not applicable for a manned aircrafts can be

---

* Project Coordinator

practical solutions for some unique UAV applications. In view of this idea a new concept for rotor blade control is introduced primarily for balancing the unequal lift distribution and for controlling hub forces. In this new concept the rotor blade lift variation is generated by a periodic trailing edge flap motions. From the aerodynamics point of view, a periodic trailing edge flap motion thought to be less disturbing for the flow field compared with a periodicly pitching airfoil.

A similar concept of changing the airfoil shape during different section of flights is applied to fixed wing aircraft. A drooped leading edge and changeable chambered wing have been designed and built for aircraft. This new wing configuration called Mission Adaptive Wing and the test aircraft have flown successfully in different sections of the mission with increased overall performances.

With this new rotor control system with minimum (or not at all) trailing edge flap motions and non-pitching rotor tips, rotor blade aerodynamic and aeroelastic problems such as:, dynamic stall, tip vortex generations can be reduced significantly. These new controls can be introduced to the rotor blades by the use of electromechanical servo and actuator systems activated and controlled by microcomputer processors. With the introduction of this new control device, a completely mechanical swashplate system can be replaced by a lighter fly-by-signal system which can be possibly achieve higher harmonic controls in an efficient and accurate manner. Beside this configurational advantages TEF control system can also reduce undesirable vortex and wake generations.

In this study, this new rotor blade control concept is analyzed up to certain complexity. As being an initial study , first of all the applicability of the trailing edge flap controls is aimed to be investigated and evaluated; rather than the complete formulation and solution of the problem.

PROBLEM FORMULATION

For the steady forward flight of the helicopter, the control inputs are calculated based on the static balance of the overall forces and moments acting on the helicopter. Periodic hub forces and moments are averaged for one blade revolution and these average values are used in the trim equations. Trim equations for a helicopter with classical pitch control is given in Reference 5. For a given helicopter configuration and system parameters, control parameters are calculated for given forward flight condition, represented by the advance ratio

$$\mu = \frac{V\cos\alpha}{\Omega R}$$

In classical rotor blade pitch control, the total pitch of the rotor blade is represented as

$$\theta = \theta_0 + \theta_{tw} r + \theta_{1s}\sin\psi + \theta_{1c}\cos\psi \qquad (2)$$

where r is the nondimensional spanwise coordinate and θtw is the built in pretwist of the rotor blade.

With the new introduced concept, the pitch motion is replaced by trailing edge flap motions with the same nature of the collective and cyclic pitch control. Flap motion can be represented by a mean and first harmonics as,

$$\Lambda = \Lambda_0 + \Lambda_{1S}\sin\psi + \Lambda_{1C}\cos\psi \qquad (3)$$

Aerodynamic forces acting on a blade element is shown in Figure 1. where L and D are sectional lift and drag forces respectively. Effective angle of attack α is given as

$$\alpha = \theta - \tan^{-1}\left(\frac{U_P}{U_T}\right) \qquad (4)$$

where θ_0 total pitch angle U_P and U_T are perpendicular and tangential sectional nondimensional velocity components respectively and given as

$$U_P = \lambda + r\dot{\beta} + \mu\beta\cos\psi$$
$$U_T = r + \mu\sin\psi \qquad (5)$$

where

$$(\dot{}) = \frac{\partial}{\partial\psi}$$

and , λ is the inflow coefficient. Flapping angle, β, is also written as

$$\beta = \beta_0 + \beta_{1c}\cos\psi + \beta_{1s}\sin\psi \qquad (6)$$

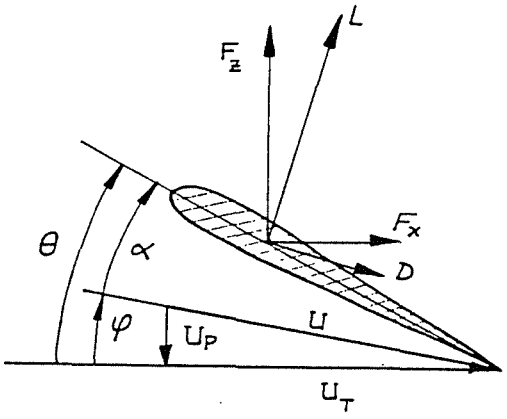

FIGURE 1. Simplified Rotor Blade Aerodynamics (Ref. 5)

With the small angle assumption and neglecting the tip loss and root cutout, the trust coefficient C_T is expressed by Johnson (5) as,

$$\frac{C_T}{\sigma a} = \frac{1}{2}\int_0^1 \hat{c}\,(U_P^2\theta - U_P U_T)\,dr \qquad (7)$$

where $\hat{c}(r)$ is the ratio of the local chord width to the average chord. Rotor solidity σ is also defined as,

$$\sigma = \frac{n_b c_{ave}}{\pi R}$$

By the use of Equations 2,5,6 and 7, trust coefficient harmonics, C_{T_0}, $C_{T_{1S}}$ and $C_{T_{1C}}$ can be written in vector form as,

$$\{C_T\} = \{C_{T0}, C_{T1S}, C_{T1C}\}^T =$$
$$\{C_T\} = [A]\{\theta\} + [C]\{\beta\} + \{q\} \qquad (8)$$

where,

$$\{\theta\} = \{\theta_0, \theta_{1S} \theta_{1C}\}^T$$

$$\{\beta\} = \{\beta_0, \beta_{1S}, \beta_{1C}\}^T$$

The matrices **A, C** and vector **q** are given Appendix.

Additional Aerodynamic Lift Due to Periodic Trailing Edge Flap Motions

A conceptual rotor blade section with periodic trailing edge flap motions is shown in Figure 2. The airfoil subject to the air stream with the rigidly set pitch angle θ_{ri}. The periodicly deflecting trailing edge flap is located with the hinge offset, Cf c/2 from the midchord. The periodic trailing edge flap motion is expressed as,

$$\Lambda = \Lambda_0 + \Lambda_{tw} r + \Lambda_{1S} \sin\psi + \Lambda_{1C} \cos\psi \tag{9}$$

Contribution of the quasisteady aerodynamic lift due to the periodic trailing edge flap motion is given by Bisplinghoff (6) as,

$$\frac{C_T}{\sigma a} = \frac{1}{a} \int_0^1 \hat{c} \left[\frac{c}{4} (f_2 - f_3) U \dot{\Lambda} - \frac{c^2}{8} f_4 \ddot{\Lambda} + c f_1 U^2 \Lambda \right] \tag{10}$$

where c, is the nondimensional chord width, U, is the resultant free stream velocity. The coefficients f_1 , f_2, f_3 and f_4 are related with the flap configuration and are given by Reference (6) as

$$\begin{aligned} f_1 &= \sqrt{1 - c_f^2} + \cos^{-1} c_f \\ f_2 &= (1 - 2c_f)\cos^{-1} c_f + (2 - c_f)\sqrt{1 - c_f^2} \\ f_3 &= c_f \sqrt{1 - c_f^2} - \cos^{-1} c_f \\ f_4 &= c_f \cos^{-1} c_f - \frac{1}{3}(2 + c_f^2)\sqrt{1 - c_f^2} \end{aligned} \tag{11}$$

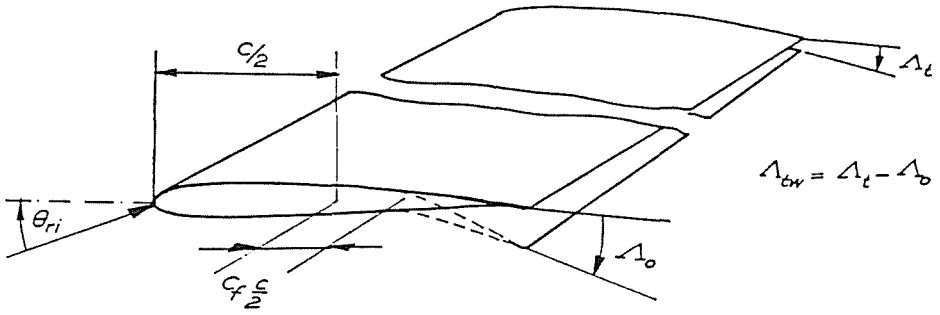

FIGURE 2. Rotor Blade Configuration With TEF Control.

Trust coefficients due to the periodic flapping motion for rotor blade with varying chord and trailing edge flap width can be derived by the use of Equations 5,6,9,10 and 11 as

$$\left\{C_{T1}^{\Lambda}\right\} = [B]\{\Lambda\} + \{q_{\Lambda}\} \tag{12}$$

where the rotor blade is assumed to be flapping up and down around the hub flapping hinge with the same flapping harmonics β of the rotor with standard pitch controls The additional

thrust coefficient harmonics due to the aerodynamic lift generated by rigid angle of attack θ_{r_1} of the rotor blade with spanwisely varying pretwist θ_{tw} can be written by the use of Equation 8 as,

$$\{C_{T2}^{\Lambda}\} = [C]\{\beta\} + \{q_{\theta}\} \tag{13}$$

The total trust harmonics of the blade with periodic trailing edge flap motions can be written in terms of Equations (12) and (13) as

$$\{C_T^{\Lambda}\} = \{C_{T1}^{\Lambda}\} + \{C_{T2}^{\Lambda}\}$$
$$\{C_T^{\Lambda}\} = [B]\{\Lambda\} + [C]\{\beta\} + \{q_{\Lambda}\} + \{q_{\theta}\} \tag{14}$$

With this new blade control variables, $\{\Lambda\}$ the first requirement is to maintain the same periodic trust variation generated by the rotor with pitch control. The equality of the trust coefficients for pitching and edge flapping controlled flight cases gives the the equation constitutes the rotor trailing edge flap control inputs;

$$[B]\{\Lambda\} = [A]\{\theta\} + \{q\} - \{q_{\Lambda}\} - \{q_{\theta}\} \tag{15}$$

Solution of equation (14) for the desired blade and flight conditions gives corresponding trailing edge flap motion harmonics which are replaced to achieve the the equivalent control conditions.

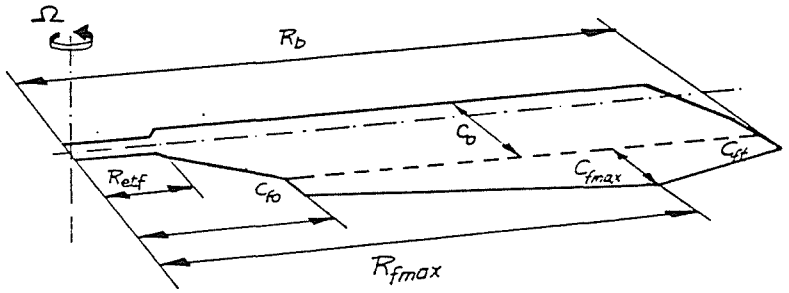

FIGURE 3. Rotor Blade With Variable TEF Configuration

RESULTS AND DISCUSSIONS

In this section, results for trailing edge flap (TEF) controls will be presented. As indicated in the introduction, only the preliminary evaluation of this new control system is aimed. Therefore certain assumptions are made to simplify the the problem. Additional to the assumptions made in formulations and the derivation of standard helicopter trim equations given in Reference 6. It is also assumed that rotor blade with TEF control is flapping in identical to the corresponding blade with pitch control.

As the initial step, a simplified conceptual design for a remotely controlled helicopter is made. Calculated design values and dimensions are given in Table 1. Secondly, standard trim calculations are performed for the simplified UAV helicopter configuration. For the blade blade configuration, relatively fast rotating rotor blade as Ω=70 rad/sec with rotor radius r= 7.5 ft is considered for the sample problem. Variations of collective pitch setting θ_o and main rotor power coefficient Cp with respect to the advance ratio μ illustrated in Figure 4, where for advance ratio μ=.25 Vcr= 77,7 knts flight conditions the lowest power setting is

achieved Pitch control harmonics for the selected blade and UAV helicopter configuration are shown in Figures 5.a-b.

TABLE 1. Basic Configuration Parameters of the Selected UAV Helicopter

Wg= 800. lb	Rtr=2.0 ft	H=1.8 ft
Rmr=7.5 ft	Ωtr=160 rad/sec	Xcg=.125 ft
Ωmr=70 rad/sec	Htr=0.	Ltr=9.375 ft

Rotor blade TEF geometries are considered in two main groups, as the first case, a uniform flap along the blade is used. For two different control cases, the total blade areas are kept same in each rotor blade configurations. First set of results are obtained for different flap hinge offsets from the midcord as Cf = .08 , .23 , and .52 respectively. In these ETF configurations, flap pretwist θtw is set equal to zero and a rigid pitch setting θn= 0.03 is used to contribute to the main rotor lift. The required periodic flap angle controls for each flap widths are compared with the cyclic pitch controls are shown in figures 6.a-c. As seen from the figures, the required cyclic ETF controls are significantly increased as the flap width decreased and higher flap controls are required for advance ratios exceeding .3 for every flap configurations.

For the UAV low power setting cruising requirement, advance ratio μ= 0.25 is selected and the corresponding cyclic flap controls were in the same range of cyclic pitch control input values. Sectional lift variations on the rectangular blade for one blade revolution are shown in Figures 7.a and 7.b. The required cyclic pitch and TEF motions are illustrated in Figures 8. Spanwise distribution of the vertical aerodynamic force at different azimuth positions are shown in Figures 9.a-b.

As seen from figures 7.a-b and 9 a-d, higher lift is achieved by TEF at the outer portion of the blade where less lift is obtained around the inner part compared with the lift generated by classical cyclic pitch control.

Based on the lift distributions obtained by the uniform TEF, rectangular flap, a spanwisely varying flap width is considered for the second group of results. In this second flap configuration, the flap width is set an initial value Cfo at r=Rb where aerodynamic lift generating part of the blade is started. Flap width reaches to its maximum value at blade radius r = Rfmax and its value reduced to Cft at the blade tip. Flap width changed linearly between these radius locations. Blade configuration is also shown in Figure 3. Rotor blades with different maximum flap locations are considered and the total required cyclic flap controls for each flap configurations are calculated. The total blade and flap areas are kept same for each configuration. The results are tabulated in Table 2 and amplitude of the periodic flap motions and the mean flap settings are decreased as the location of the maximum flap width is set closer to the rotor tip.

TABLE 2. Amplitude of The Periodic TEF Controls for Different Triangular Flaps

Flap Planeform		Amplitude of the Periodic TEF Controls (deg)
Rectangular		3.56
Triangular	Rfmax=.3	4.77
	Rfmax=.5	4.06
	Rfmax=.7	3.48
	Rfmax=.9	2.98

Lift distributions both for TEF and pitch control cases on different triangular an rectangular flap geometries are shown in Figures 10 and 11 respectively. As the maximum flap location set closer to the blade tip, the peaks of the lift distributions are shifted towards the blade location with higher flap widths. Since the blade planeform area is kept same in each case, similar variations in the blade sectional lifts are also observed for the pitch control cases.

Spanwise lift distributions for both control cases and for different triangular flap configurations as Rfmax=.9, .7 and .3 are illustrated in Figures 12.a-c and 13.a-c for azimuth locations ψ=90 and ψ=180 respectively. In general lift distribution patterns generated by the

blade control systems and by TEF control, slightly higher sectional lifts are obtained around the maximum flap location whereas pitch control generated comparably higher lifts in the inner portion of the rotor blade.

As observed, TEF control achieved identical rotor blade trust controls compared to the corresponding pith controlled blade. Based on this conclusion further studies have been initiated to model and analyze the TEF control concept. Related undergoing research studies are as follows;

- Derivation and the solution of special trim equations specific to very light UAV rotary wing aircraft,
- Response and stability analysis of elastic hingeless rotor blade with highly elastic TEF,
- Optimum design of the TEF geometry and frequency placement to avoid air resonances and instabilities.

APPENDIX

$$[A]=\begin{bmatrix} \frac{C_{12}}{2}+C_{10}\frac{\mu^2}{4} & C_{11}\frac{\mu}{2} & 0 \\ C_{11}\frac{\mu}{2} & \frac{C_{12}}{2}+C_{10}\frac{3\mu^2}{8} & 0 \\ 0 & 0 & \frac{C_{12}}{2}+C_{10}\frac{\mu^2}{8} \end{bmatrix} \quad [B]=\begin{bmatrix} d_{3k2}+d_{3k0}\frac{\mu^2}{2} & d_{3k1}\mu & -d_{1k0}\frac{\mu}{2} \\ 0 & d_{2k0}+d_{3k2}+d_{3k0}\frac{3\mu^2}{4} & -d_{1k1} \\ 0 & d_{1k1} & d_{3k0}+d_{3k2}+d_{3k0}\frac{\mu^2}{4} \end{bmatrix}$$

$$[C]=\begin{bmatrix} 0 & 0 & 0 \\ 0 & 0 & \frac{C_{12}}{2}-C_{10}\frac{\mu^2}{8} \\ -C_{11}\frac{\mu}{2} & -\frac{C_{12}}{2}-C_{10}\frac{\mu^2}{8} & 0 \end{bmatrix}$$

$$\begin{Bmatrix} q \\ \theta \end{Bmatrix}=\begin{Bmatrix} \left(\frac{C_{12}}{2}+C_{10}\frac{\mu^2}{4}\right)\theta_{1I}-C_{11}\frac{\lambda}{2}+\left(\frac{C_{13}}{2}+C_{11}\frac{\mu^2}{4}\right)\theta_{tw}^{\Lambda} \\ C_{11}\mu\,\theta_{1I}-C_{10}\frac{\mu\lambda}{2}+C_{12}\mu\,\theta_{tw}^{\Lambda} \\ 0 \end{Bmatrix} \quad \{q\}=\begin{Bmatrix} -C_{11}\frac{\lambda}{2}+\left(\frac{C_{13}}{2}+C_{11}\frac{\mu^2}{4}\right)\theta_{tw} \\ -C_{10}\frac{\mu\lambda}{2}+C_{12}\mu\,\theta_{tw} \\ 0 \end{Bmatrix} \quad \{q_\Lambda\}=\begin{Bmatrix} \left(d_{3k3}+d_{3k1}\frac{\mu^2}{2}\right)\Lambda_{tw} \\ 2d_{3k2}\,\mu\,\Lambda_{tw} \\ 0 \end{Bmatrix}$$

$$d_{1k}=\frac{c}{4a}(f_2-f_3),\quad d_{2k}=\frac{c^2}{8a}f_4,\quad d_{3k}=\frac{1}{2}f_1$$

$$d_{1k0}=\int_0^1 \hat{c}\,d_{1k}\,dr,\quad d_{1k1}=\int_0^1 \hat{c}\,r\,d_{1k}\,dr$$

$$d_{2k0}=\int_0^1 \hat{c}\,d_{2k}\,dr$$

$$d_{3k0}=\int_0^1 \hat{c}\,d_{3k}\,dr,\quad d_{3k1}=\int_0^1 \hat{c}\,r\,d_{3k}\,dr,\quad d_{3k2}=\int_0^1 \hat{c}\,r^2 d_{3k}\,dr,\quad d_{3k3}=\int_0^1 \hat{c}\,r^3 d_{3k}\,dr$$

$$C_{10}=\int_0^1 \hat{c}\,dr,\quad C_{11}=\int_0^1 \hat{c}\,r\,dr,\quad C_{12}=\int_0^1 \hat{c}\,r^2 dr,\quad C_{13}=\int_0^1 \hat{c}\,r^3 dr$$

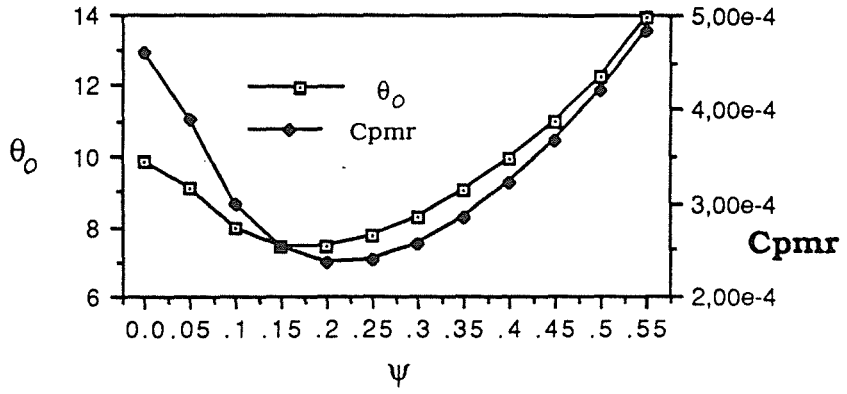

FIGURE 4: Collective Pitch and Power Coefficient Variation for the UAV helicopter Configuration.

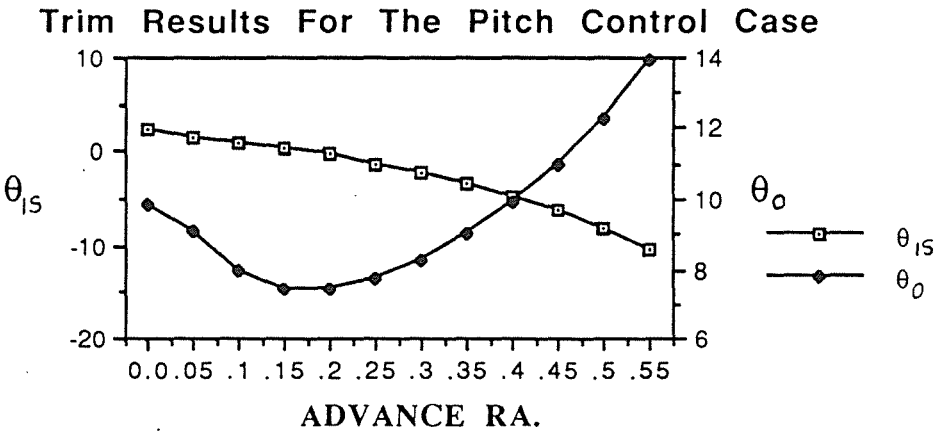

FIGURE 5.a: Trim Solutions; θo and θis variations

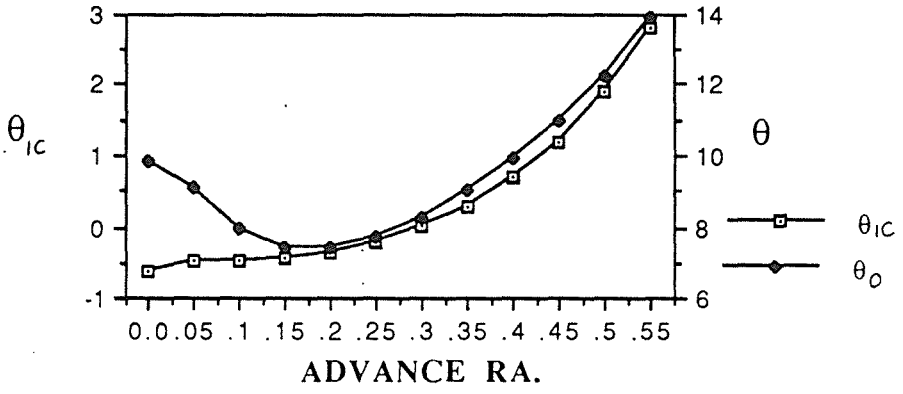

FIGURE 5.b: Trim Solutions; θo and θic Variation.

TEF Control Inputs For Different Flap Widths

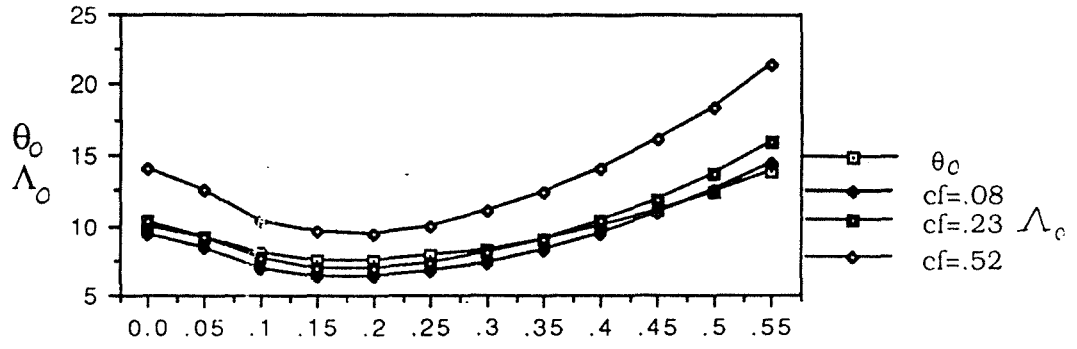

Advance Ratio.
FIGURE 6.a

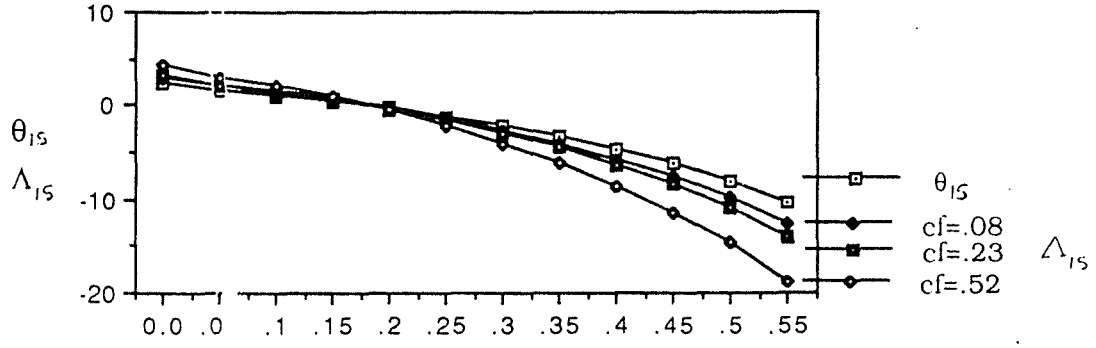

Advance Ratio
FIGURE 6.b

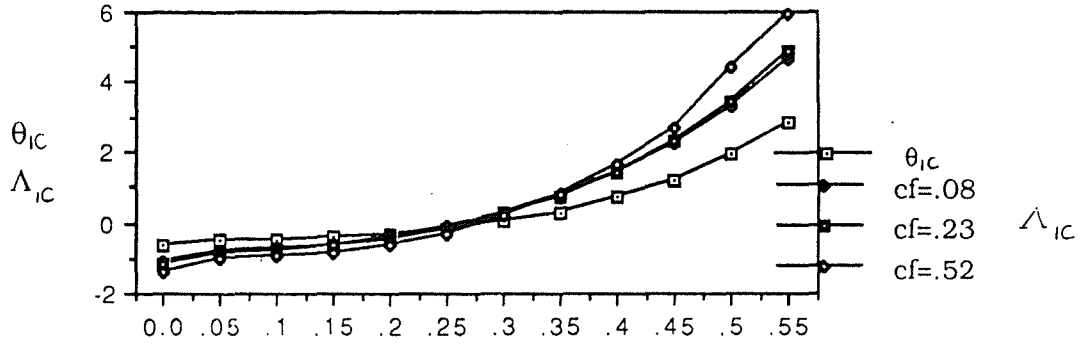

Advance Ratio
FIGURE 6.c

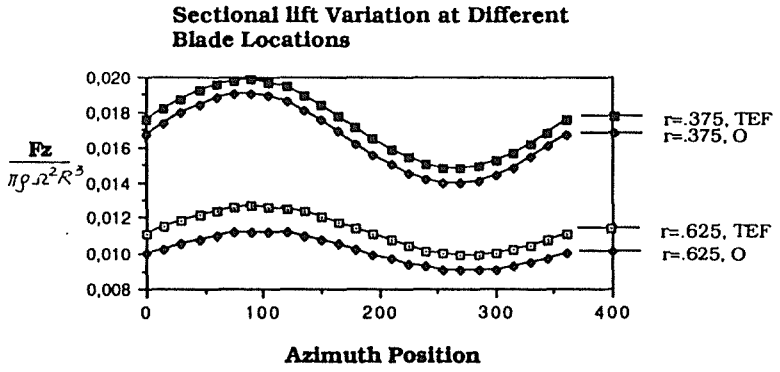

FIGURE 7.a: Variation of the Sectional Lift at r=.375 and .625

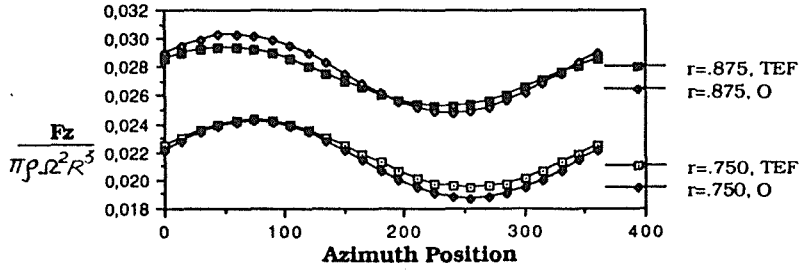

FIGURE 7.b: Variation of the Sectional Lift at r=.750 and .875

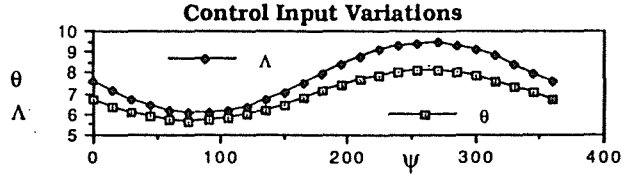

FIGURE 8: Control Input Variations

17th European Rotorcraft Forum
September 24-26, 1991 Berlin, Germany

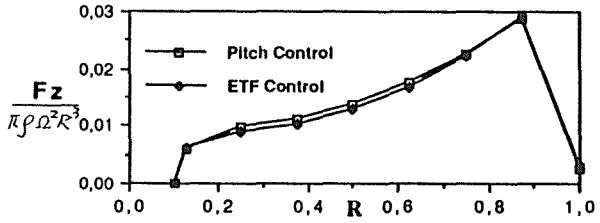

FIGURE 9.a: Sectional Lift Distribution On The Rectangular Blade at ψ=0°

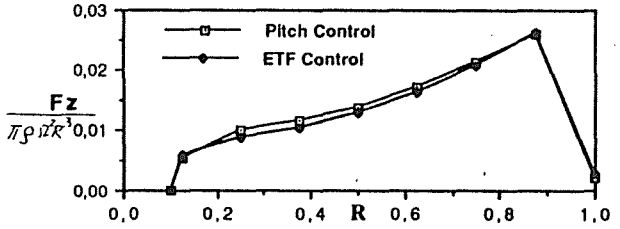

FIGURE 9.b: Sectional lift Distribution on the Rectangular Blade at ψ=180°

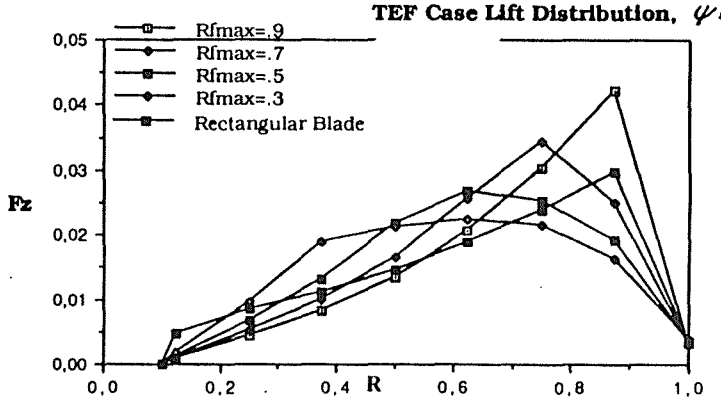

FIGURE 10: Sectional Lift Distribution for TEF Control Case on the Triangular Blade with Different Maximum Flap Locations at ψ=90°

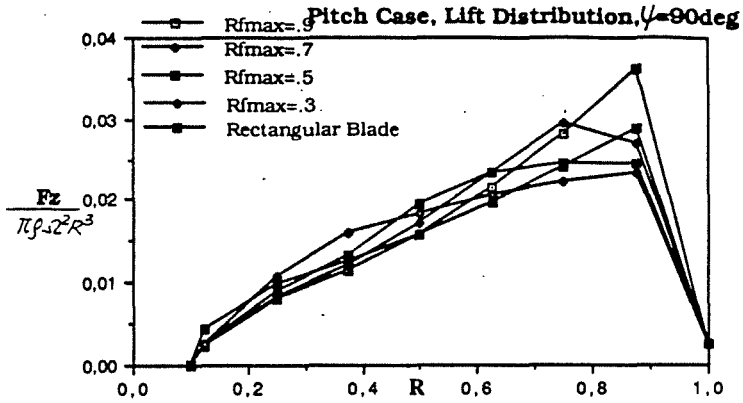

FIGURE 11: Sectional Lift Distribution for Pitch Control Case, Triangular Blade with Different Maximum Flap Locations at ψ=90

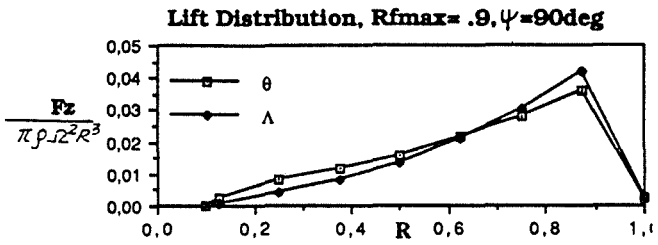

FIGURE 12.a: Lift Distribution on Triangular Blade Rfmax=.9 at ψ=90.

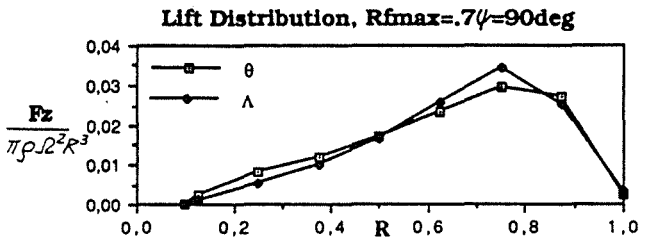

FIGURE 12.a: Lift Distribution on Triangular Blade Rfmax=.7 at ψ=90.

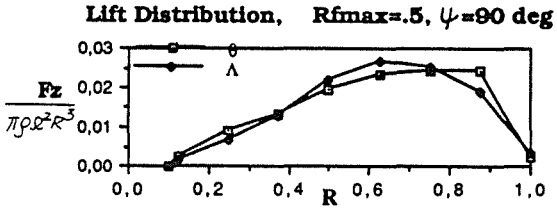

FIGURE 12.a: Lift Distribution on Triangular Blade Rfmax=.5 at ψ=90.

REFERENCES:

(1) Chopra, I., and Johnson, W., " Flap-lag-torsion Aeroelastic Stability of Circulation Controlled Rotors in Hover," Journal of the American Helicopter Society, Vol. 24, (2), April 1979.

(2) Watkins, C. B., Reader, K. R., and Dutta, S. K., " Pneumodynamic Characteristics of a Circulation Control Rotor Model," Journal of the American Helicopter Society , Vol. 30 (3), July 1985.

(3) Chopra, I. " Aeroelastic Stability of a Bearingless Circulation Control Rotor Blade in Hover," Journal of American Helicopter Society, Vol. 30 (4), October 1985.

(4) Chopra, I. " Aeroelastic Stability of a Bearingless Circulation Control Rotor in Forward Flight," Journal of the American Helicopter Society, Vol. 33 (3), July 1988.

5) Johnson, W., *Helicopter Theory* , Princeton University Press, Princeton, New Jersey, 1980.

(6) Bishlinghoff, R. L., Ashley, H., and Halfman, R. L., *Aeroelasticity*, Addison Wesley Publishing Company, Cambridge, Mass 1955.